EAN 2019
57th conference on experimental stress analysis

An alternative neo-Hookean material model with internal damping for finite-strain elastoplasticity

JERÁBEK Róbert[1,a] and ÉCSI Ladislav[1,b]

[1]Institute of Applied Mechanics and Mechatronics; Faculty of Mechanical Engineering; Slovak University of Technology in Bratislava; Námestie slobody 17, 812 31 Bratislava 1, Slovak Republic

[a]robert.jerabek@stuba.sk, [b]ladislav.ecsi@stuba.sk

Keywords: Nonlinear continuum theory for finite deformation of elastoplastic media, objective and thermodynamically consistent material model, Neo-Hookean material with internal damping

Abstract. At present, multiplicative plasticity theories are used to model material degradation of hyperelastic materials within the framework of finite-strain elastoplasticity. The theories assume that the intermediate configuration of the body is locally unstressed, for which no deformation exists that meets the conditions of compatibility. The assumption, however; is in contradiction to the theory of nonlinear continuum mechanics, as it violates proper stress transformations, resulting from the invariance of the internal mechanical power. As a result, the theories and their related material models are not continuum based. In this paper, an alternative neo-Hookean material model with internal damping for finite-strain elastoplasticity is presented. The model, based on the first nonlinear continuum theory of finite deformations of elastoplastic media, can imitate material degradation of the neo-Hookean material under excessive dynamic loading.

Introduction

Hyperelastic materials, such as rubber, vulcanized elastomers, various types of polymers, biomaterials, etc. are nonlinear elastic materials. The materials have a wide range of applications in industry. Hyperelastic materials can withstand large strains without undergoing permanent deformations or being fractured. The materials are considered to be isotropic under elastic loading and their constitutive equations are derived from strain energy density functions [1], defined in terms of the stored energy in the material per unit of the reference volume at each time instant [2]. In computational mechanics, there are available a number of different strain-energy functions to model hyperelastic materials. Without the need for completeness, let us mention a few concrete examples of hyperelastic materials and their applications. The Mooney-Rivlin material is used to model rubber-like materials and polymers [1], whose special case is the neo-Hookean material [1]. The Yeoh material model [3] was developed to model carbon-black filled rubber vulcanizates. The Ogden material has widespread use in modelling biomaterials and soft tissues [4, 5]. The Blatz-Ko [6] and the Arruda-Boyce [7] material models were proposed to model foamed or compressible elastomers. The Ogden-Storakers material has widespread use in modelling highly compressible foamed elastomers [8]. From among the newer materials, one should mention the Bower material [9], the Gent material [10] and the Dill material [11] for modelling rubber-like solids and polymers.

Contemporary material models for material degradation of hyperelastic materials use hyperelastic-plastic based multiplicative plasticity models to model the behaviour of the materials within the framework of finite-strain elastoplasticity. Though contemporary multiplicative plasticity models are considered to be continuum based, in reality they are not if one studies them strictly from the nonlinear continuum mechanics point of view. The theories assume that the intermediate configuration of the body is stress-free or locally unstressed, for which no deformation exists that meets the conditions of compatibility [12]. The assumption, however; is in contradiction to the theory of nonlinear continuum mechanics, as it violates proper stress transformations resulting from the invariance of the internal mechanical power.

The aim of this paper is to present a study of material degradation of a silicone specimen in uniaxial tension using a thermodynamically consistent neo-Hookean material model with internal damping. The model, which is based on the first nonlinear continuum theory of finite deformations of elastoplastic media [13], can imitate material degradation of the neo-Hookean material under excessive dynamic loading. In this paper a few selected analysis results are presented and briefly discussed.

Theory

The constitutive equation of the material. Hyperelastic materials are nonlinear elastic materials, whose constitutive equations are derived from strain energy density functions [1]. When in addition, they undergo material degradation during their mechanical loading, the materials are often modelled as elastoplastic, using the accumulated plastic strain as a measure of the material degradation. Considering the nonlinear continuum theory of finite deformations of elastoplastic media [13, 14], the elastic part of the deformation gradient can be expressed in the intermediate configuration of the modelled body as [14, 15]

$$\mathbf{F}^{el} = \mathbf{F} - \frac{\partial^0 \mathbf{u}^{pl}}{\partial \mathbf{X}}. \tag{1}$$

The definition of the left isochoric Cauchy-Green tensor is based on the Lagrangian multiplicative split of the elastic deformation gradient $\mathbf{F}^{el}$ into a volumetric part $\mathbf{F}^{el}_{vol}$ and an isochoric part $\mathbf{F}^{el}_{iso}$. The left elastic isochoric Cauchy-Green tensor then takes the form [1, 12]

$$\mathbf{B}^{el}_{iso} = \mathbf{F}^{el}_{iso} \cdot \left(\mathbf{F}^{el}_{iso}\right)^T = \det\left(\mathbf{F}^{el}\right)^{-\frac{2}{3}} \cdot \mathbf{B}^{el}. \tag{2}$$

Since the material remains elastic in the intermediate configuration, there is no need to modify its strain energy density function. In this research neo-Hookean material model is used to model the plastic behaviour of hyperelastic-plastic material, whose strain energy density function takes the following well-known form [12, 13]

$$\overline{\psi}^*\left(I_1^*, J^{el}\right) = G \cdot \left(I_1^* - 3\right) + \frac{1}{d} \cdot \left(J^{el} - 1\right)^2, \tag{3}$$

where $I_1^* = I_1^*\left(\mathbf{B}^{el}_{iso}\right) = tr\left(\mathbf{B}^{el}_{iso}\right)$ is the first invariant of the characteristic equation of the corresponding eigenvalue problem using the left isochoric Cauchy-Green deformation tensor $\mathbf{B}^{el}_{iso}$ and $J^{el} = \det\left(\mathbf{F}^{el}\right)$ is the Jacobian of elastic deformation. The model uses two material

parameters, the shear modulus G and a parameter d, which controls bulk compressibility. If d is zero, the material is incompressible. The relationship between the bulk modulus and the parameter d is then defined as [1]

$$K = \frac{2}{d}, \tag{4}$$

where the former can also be expressed in terms of the shear modulus G and the Poisson's ratio ν of the material as follows [16]

$$K = \frac{2 \cdot G \cdot (1+\nu)}{3 \cdot (1-2 \cdot \nu)}. \tag{5}$$

The stress constitutive function of the material in the intermediate configuration of the body then can be expressed as a Kirchhoff stress measure in the form

$$\boldsymbol{\tau}^{el} = \frac{\partial \overline{\psi}^{*}}{\partial \mathbf{F}^{el}} \bullet \left(\mathbf{F}^{el}\right)^{T} = G \cdot dev\left[\mathbf{B}_{iso}^{el}\right] + \frac{2}{d} \cdot J^{el} \cdot \left(J^{el} - 1\right) \cdot \mathbf{I}, \tag{6}$$

where the deviator of the left elastic isochoric Cauchy-Green tensor is defined as

$$dev\left[\mathbf{B}_{iso}^{el}\right] = \mathbf{B}_{iso}^{el} - \frac{tr\left(\mathbf{B}_{iso}^{el}\right)}{3} \cdot \mathbf{I}. \tag{7}$$

The corresponding elastic 2nd Piola-Kirchhoff stress tensor then takes the form [14, 17]

$$\mathbf{S}^{el} = \left(\mathbf{F}^{el}\right)^{-1} \cdot \boldsymbol{\tau}^{el} \cdot \left(\mathbf{F}^{el}\right)^{-T}. \tag{8}$$

In order to take into account the internal/material damping, the material model is modified as follows

$$\mathbf{S} = \mathbf{S}^{el} + \mathbf{S}^{vis} = \left(\mathbf{F}^{el}\right)^{-1} \cdot \boldsymbol{\tau}^{el} \cdot \left(\mathbf{F}^{el}\right)^{-T} + {}^{mat}\mathbb{C}^{vis} : {}^{*}\dot{\mathbf{E}}^{el} \tag{9}$$

where ${}^{*}\dot{\mathbf{E}}^{el}$ is the time derivative of the elastic Green-Lagrangian strain tensor, derived from the elastic deformation gradient (Eqn. (1)) as follows [17]

$${}^{*}\dot{\mathbf{E}}^{el} = \frac{1}{2} \cdot \left[\left(\dot{\mathbf{F}}^{el}\right)^{T} \cdot \mathbf{F}^{el} + \left(\mathbf{F}^{el}\right)^{T} \cdot \dot{\mathbf{F}}^{el}\right], \tag{10}$$

and ${}^{mat}\mathbb{C}^{vis}$ is the fourth order material viscosity tensor, which can be calculated using the following formula

$${}^{mat}\mathbb{C}^{vis} = 2 \cdot G^{vis} \cdot \mathbb{I} + \lambda^{vis} \cdot \mathbf{I} \otimes \mathbf{I}, \tag{11}$$

$$G^{vis} = \frac{E^{vis}}{2 \cdot \left(1+\upsilon^{vis}\right)}, \quad \lambda^{vis} = \frac{\upsilon^{vis} \cdot E^{vis}}{\left(1+\upsilon^{vis}\right) \cdot \left(1-2 \cdot \upsilon^{vis}\right)}. \tag{12}$$

In Eqns. (11), (12) G^{vis} is the viscous shear modulus, λ^{vis} is the viscous Lamé constant, $\mathbb{I}$ denotes the symmetric fourth-order identity tensor, $\mathbf{I}$ is the second-order identity tensor, E^{vis} is the viscous Young's modulus and υ^{vis} is the viscous Poisson's ratio.

The stress constitutive function of the modified neo-Hookean material with internal damping then takes its final form in the current configuration as

$$\boldsymbol{\tau} = \mathbf{F}\cdot\mathbf{S}\cdot\mathbf{F}^T = \mathbf{F}\cdot\left[\left(\mathbf{F}^{el}\right)^{-1}\cdot\boldsymbol{\tau}^{el}\cdot\left(\mathbf{F}^{el}\right)^{-T} + {}^{mat}\mathbb{C}^{vis} : {}^{*}\dot{\mathbf{E}}^{el}\right]\cdot\mathbf{F}^T. \tag{13}$$

The reference definition of the yield surface. In this study J_2 plasticity with isotropic hardening was considered. The yield surface in the material model was defined in the Kirchhoff stress space as follows [16, 17]

$${}^{\tau}\psi = {}^{\tau}\sigma_{eq}\left(\boldsymbol{\tau}\right) - \tau_y \le 0, \tag{14}$$

where the von-Mises equivalent Kirchhoff stress is defined as

$${}^{\tau}\sigma_{eq}\left(\boldsymbol{\tau}\right) = \sqrt{\frac{3}{2}\cdot\sum\boldsymbol{\tau} : \sum\boldsymbol{\tau}}, \qquad \sum\boldsymbol{\tau} = \boldsymbol{\tau} - \frac{tr\left(\boldsymbol{\tau}\right)}{3}\cdot\mathbf{I}. \tag{15}$$

In Eqn. (14) τ_y denotes the Kirchhoff yield stress, which in the analysis was expressed as

$$\tau_y = \sqrt{r^2 - \left(a\cdot\frac{\partial^0 u^{pl}_{UT11}}{\partial X}\right)^2}, \quad r = {}^{\tau}\tau_y + {}^{\tau}Q, \quad center = \sqrt{r^2 - {}^{\tau}\tau_y^2}, \quad a = \frac{center + r}{b}, \tag{16}$$

where ${}^{\tau}\tau_y$ is the constant yield stress and ${}^{\tau}Q$ is the maximum hardening stress. Here, the parameter $\partial^0 u^{pl}_{UT11}/\partial X$ controls the material hardening/softening. It stands for the axial component of the material gradient of the Lagrangian plastic displacement field and is determined during uniaxial tensile testing of the material. In Eqn. (16) b denotes the maximum value of $\partial^0 u^{pl}_{UT11}/\partial X$, at which the material loses its integrity, i.e. when $\tau_y = 0$. In Eqn. (17) the spatial and the material gradients of the plastic velocity field are defined as follows, where $\mathbf{N}$ is a unit outward normal of the yield surface and $\dot{\lambda}$ is the plastic multiplier [14, 15]

$$\frac{\partial\dot{\mathbf{u}}^{pl}}{\partial\mathbf{x}} = \mathbf{d}^{pl} = \dot{\lambda}\cdot\frac{\partial^{\tau}\Psi}{\partial\boldsymbol{\tau}} = \dot{\lambda}\cdot\sqrt{\frac{3}{2}}\cdot\mathbf{N}, \quad \mathbf{N} = \frac{\boldsymbol{\Sigma}\boldsymbol{\tau}}{\left\|\boldsymbol{\Sigma}\boldsymbol{\tau}\right\|} = \frac{\boldsymbol{\Sigma}\boldsymbol{\tau}}{\sqrt{\boldsymbol{\Sigma}\boldsymbol{\tau} : \boldsymbol{\Sigma}\boldsymbol{\tau}}}, \quad \frac{\partial^0\dot{\mathbf{u}}^{pl}}{\partial\mathbf{X}} = \dot{\lambda}\cdot\sqrt{\frac{3}{2}}\cdot\mathbf{N}\cdot\mathbf{F}. \tag{17}$$

The corresponding formulas at a material point of the specimen during uniaxial tensile testing of the material then can be determined as

$$\frac{\partial\dot{u}^{pl}_{UT11}}{\partial x} = \dot{\lambda}\cdot\sqrt{\frac{3}{2}}, \quad \frac{\partial^0\dot{u}^{pl}_{UT11}}{\partial X} = \frac{\partial\dot{u}^{pl}_{UT11}}{\partial x}\cdot F_{UT11} = \dot{\lambda}\cdot\sqrt{\frac{3}{2}}\cdot F_{UT11}, \quad \frac{\partial^0 u^{pl}_{UT11}}{\partial X} = \int_0^t\frac{\partial^0\dot{u}^{pl}_{UT11}}{\partial X}\cdot dt. \tag{18}$$

In the analysis, numerical uniaxial tensile testing was used to assess the values of the elastic deformation gradient $\mathbf{F}_{UT}^{el}$, the axial component of the elastic deformation gradient F_{UT11}^{el}, the Jacobian of the elastic deformation gradient J_{UT}^{el} and the deformation gradient $\mathbf{F}_{UT}$ of the modelled material. Normally these would be determined experimentally, but since contemporary tensile testing does not provide the time-histories of the variables, we used the following formulas to determine them numerically [14, 15]

$$\begin{aligned} \mathbf{F}_{UT}^{el} &= diag\left[F_{UT11}^{el}, \quad 1, \quad 1\right], F_{UT11}^{el} = F_{UT11} - \frac{\partial^0 u_{UT11}^{pl}}{\partial X}, \\ J_{UT}^{el} &= \det\left(\mathbf{F}_{UT}^{el}\right), \mathbf{F}_{UT} = diag\left[F_{UT11}, \quad 1, \quad 1\right]. \end{aligned} \tag{19}$$

Then during the analysis, the numerical uniaxial tensile testing too was realized by solving the following equation

$$\tau_{UT11} - \tau_y = 0. \tag{20}$$

Here τ_{UT11} is the axial component of the $\boldsymbol{\tau}_{UT} = \boldsymbol{\tau}$ stress constitutive function of the material defined by Eqn. (13), in which the deformation gradient $\mathbf{F}$ is replaced by $\mathbf{F}_{UT}$ and the elastic deformation gradient $\mathbf{F}^{el}$ by $\mathbf{F}_{UT}^{el}$. There was no change in the definition of the yield stress τ_y.

Numerical experiment

As a numerical experiment, material degradation of a silicone specimen in uniaxial tension was studied. The specimen dimensions were $0.05\text{m} \times 0.05\text{m} \times 0.6\text{m}$. The elastic material properties of the neo-Hookean material model were determined by the collective K.B. Putra et. al. [18]. One end of the specimen was fixed, while the second end underwent axial deformation by imposing tensile surface traction on it as a product of constant $p = 0.5\ MPa$ pressure and a Heaviside step function. In order to model the grip of the testing machine, the specimen was guided in transversal directions by imposing zero displacements in X and Y directions at its moving end as shown in Fig. 1. The figure also shows the spatially discretized body of the specimen where the arrows indicate the loading.

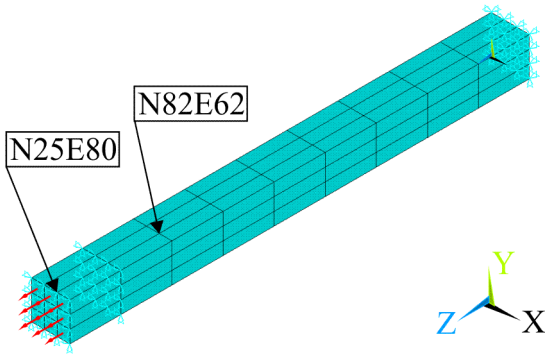

Fig. 1: Spatially discretized specimen in the analysis

The specimen was initially at rest. The analysis was run as transient dynamic until it failed to converge using implicit time integration and a $0.00001\ s$ time step size. Table 1 outlines the material properties of the specimen used in the finite element analysis.

Table 1: The material properties of the silicone specimen

$\rho_0 \left[kg \cdot m^{-3} \right]$	1520
$G \left[Pa \right]$	229 600
$d \left[- \right]$	0.00000624054
$E^{vis} \left[Pa \cdot s \right]$	7310
$\upsilon^{vis} \left[- \right]$	0.33
${}^{\tau}\tau_y \left[Pa \right]$	350 000
${}^{\tau}Q \left[Pa \right]$	50 000
$b \left[- \right]$	2.0

Numerical results

Fig. 2 shows a few selected results at the end of the numerical analysis. These are the axial displacement distribution, the accumulated plastic strain distribution, the 1st principal stress distribution as a Cauchy's stress measure, the von Mises stress distribution as a Cauchy's stress measure, the parameter $\partial^0 u^{pl}_{UT11} / \partial X$ and the axial component of the deformation gradient F_{UT11} at the end of the analysis in the current configuration of the body. The values of the parameter $\partial^0 u^{pl}_{UT11} / \partial X$ and of the axial component of the deformation gradient F_{UT11} are calculated from the numerical tensile test of the material.

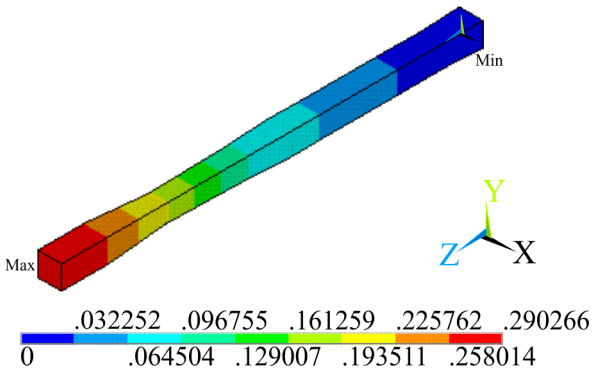

Axial displacement field $\left[m \right]$

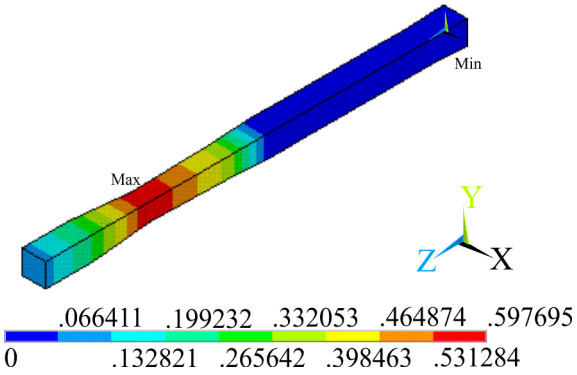

Accumulated plastic strain distribution $\left[- \right]$

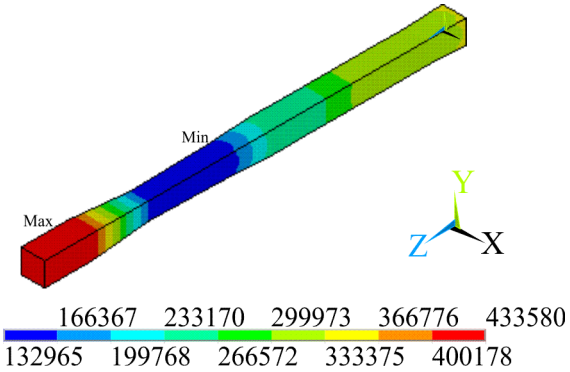

1st principal stress distribution $\left[Pa \right]$

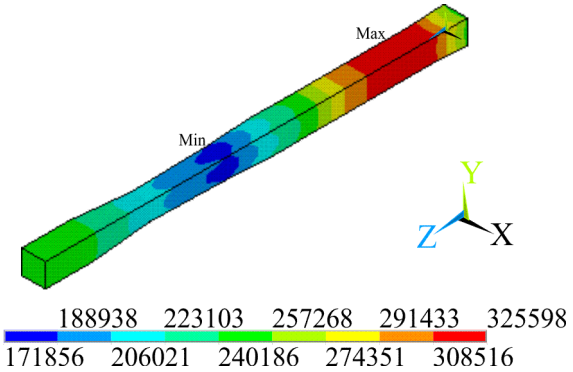

von Mises stress distribution $\left[Pa \right]$

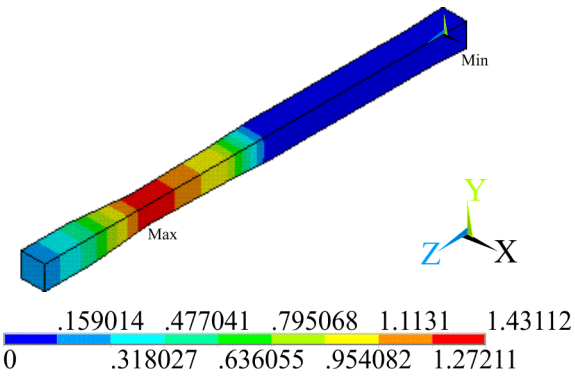

Parameter $\partial^0 u^{pl}_{UT11} / \partial X$ [−]

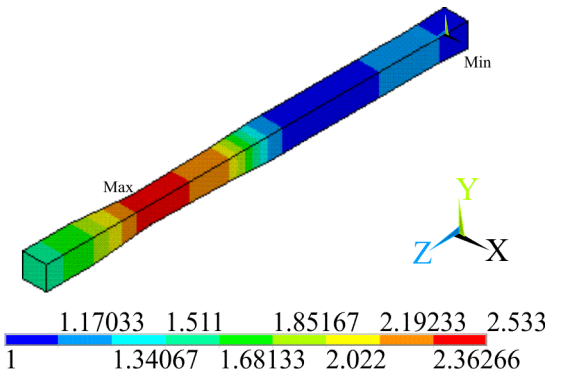

Axial component of the deform. gradient [−]

Fig. 2: A few selected results at the end of the analysis

As can be seen in the above figure, the maximum axial displacement of the moving end is $0.29\ m$ at the end of the analysis, i.e. when the analysis stopped to convergence. The maximum elongation is 48.3 %, which approximately corresponds to 60 % of the accumulated plastic strain and 143 % of the parameter $\partial^0 u^{pl}_{UT11} / \partial X$ that controls the isotropic hardening process. The axial component of the deformation gradient coming from the numerical uniaxial tensile test of the material is about 2.53 at the end of the analysis.

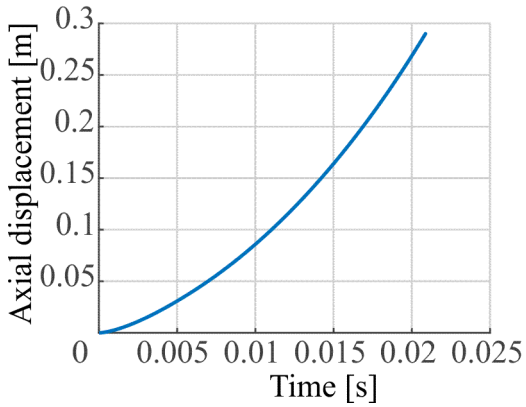

Axial displacement time-history curve at node *N25E80*

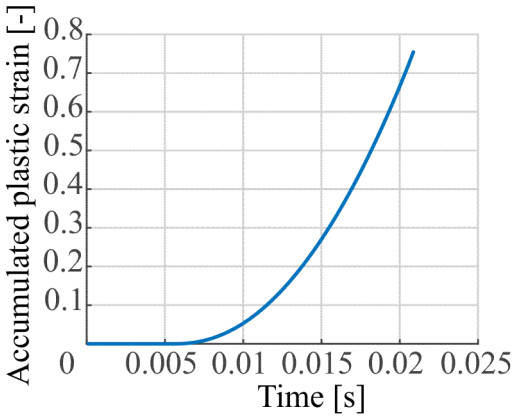

Accumulated plastic strain time-history curve at node *N82E62*

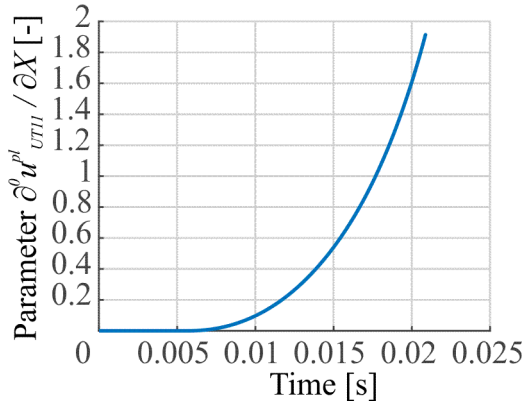

The time-history curve of the parameter $\partial^0 u^{pl}_{UT11} / \partial X$ at node *N82E62*

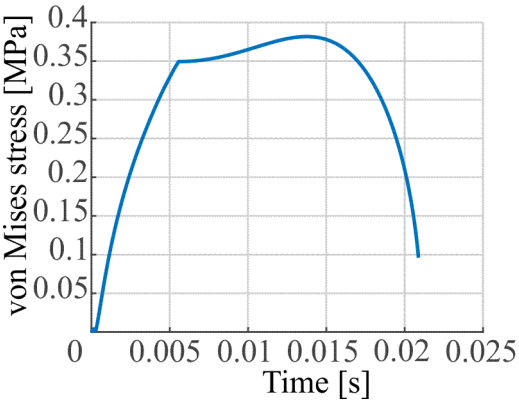

von Mises stress time-history curve at node *N82E62*

Fig. 3: A few selected time-history curves

Fig. 3 depicts a few selected time-history curves. These are the axial displacement time-history curve at node *N25* of element *E80* at the moving end of the specimen, the accumulated plastic strain time-history curve, the time-history curve of the parameter $\partial^0 u^{pl}_{UT11} / \partial X$ and the von Mises stress time-history curve at node *N82* of element *E62*. The locations of the nodes *N25E80* and *N82E62* are depicted in Fig. 1. As can be seen in the above figure, the material degradation starts approximately at $0.0056\ \mathrm{s}$ and continues until the end of the analysis, which can distinctly be seen in the time-history curves of the accumulated plastic strain and the parameter $\partial^0 u^{pl}_{UT11} / \partial X$ respectively. Similarly, the von Mises stress value rapidly increases in elastic loading and also during material hardening, but at a decreasing pace in the hardening stage. When the stress reaches its maximum at $0.014\ \mathrm{s}$, i.e. when the maximum load-carrying capacity of the body has been reached, the von Mises stress starts to decrease until the analysis fails to converge. Such behaviour, shown on the von-Mises stress time-history curve of the Cauchy's stress of the neo-Hookean material, is characteristic of all materials under excessive loading. Material softening is caused by internal damaging processes in the material, which in phenomenological numerical analyses are taken into account by the uniaxial stress-strain curve of the material.

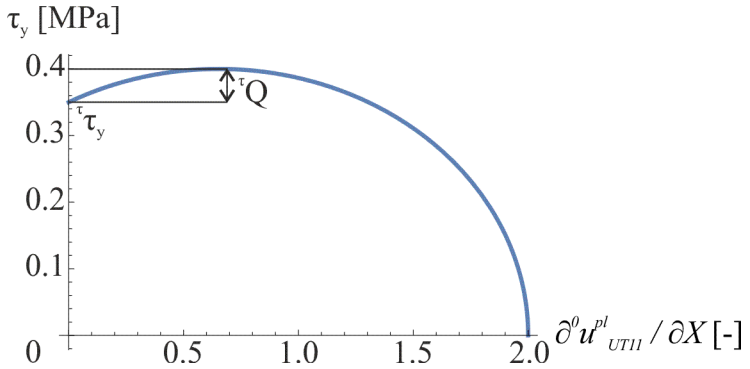

Fig. 4: The uniaxial Kirchhoff stress-strain curve of the material

Fig. 4 shows the uniaxial stress-strain curve of the neo-Hookean material used in the analysis. As it was mentioned in the above, the parameter $\partial^0 u^{pl}_{UT11} / \partial X$ controls the hardening/softening process. When its value exceeds 0.6, the material softens.

It also should be noted that the von Mises stress and the 1st principal stress values as Cauchy's stress measures are lower than their values as Kirchhoff stress measures. This is due to the fact that the Jacobian of deformation is $J > 1$ during the whole loading process, where considering that $\boldsymbol{\sigma} = \boldsymbol{\tau} / J$, caused the aforementioned decrease [15].

Conclusions

In this research uniaxial tension of a silicone specimen under dynamic loading was studied using a modified neo-Hookean material model with internal damping. The material model is based on the first continuum theory for finite deformations of elastoplastic media, which allows for the development of objective and thermodynamically consistent material models. The results of such material models are independent of the model description and the particularities of the model formulation. Although our analysis results seem to be reasonable, the proper verification of the model requires thorough material testing in order to determine all material parameters of the presented neo-Hookean material model. In addition to this, uniaxial tensile testing has to be extended by deformation gradient determination, which in general is not the subject of current material testing procedures.

References

[1] R.M. Hackett, Hyperelasticity primer, Springer, NY, 2016.

[2] A. Ali, M. Hosseini, B. Sahari, A review of constitutive models for rubber-like materials, American Journal of Engineering and Applied Sciences. 3 (2010) 1:232–239.

[3] O.H. Yeoh, Characterization of Elastic Properties of Carbon-black-filled rubber vulcanizates, Rubber Chem. Technol. 63 (1990) 792–805.

[4] R.W. Ogden, Non-Linear Elastic Deformations, Chichester, Ellis Horwood, 1984.

[5] R.W. Ogden, Large Deformation Isotropic Elasticity – On the Correlation of Theory and Experiment for Incompressible Rubberlike Solids, Proc. R. Soc. Lond. A, 326 (1972) 565–584.

[6] P.J. Blatz, W.L. Ko, Application of Finite Elasticity to the Deformation of Rubbery Materials, Trans. Soc. Rheol. 6 (1962) 223–251.

[7] E.M. Arruda, M.C. Boyce, Three-dimensional Constitutive Model for the Large Stretch Behavior of Rubber Elastic Materials, J. Mech. Phys. Solids. 41 (1993) 389–412.

[8] B. Storakers, On material representation and constitutive branching in finite compressible elasticity, J. Mech. Phys. Solids. 34 (1986) 125-145.

[9] A.F. Bower, Applied Mechanics of Solids, CRC, Boca Raton, 2010.

[10] A.N. Gent, A New Constitutive Relation for Rubber, Rubber Chem. Technol. 69 (1996) 59-61.

[11] E.H. Dill, Continuum Mechanics: Elasticity, Plasticity, Viscoelasticity, CRC, Boca Raton, 2007.

[12] E.A. de Souza Neto, D. Perić, D.R.J. Owen, Computational methods for plasticity, Theory and applications, John Wiley & Sons Ltd., Singapore, 2008.

[13] L. Écsi, P. Élesztős, An alternative material model using a generalized J2 finite-strain flow plasticity theory with isotropic hardening, Int. J. Applied Mechanics and Engineering, 23 (2018) 2:351-365

[14] L. Écsi, P. Élesztős, An Alternative Method for Modelling the Degradation of Hyperelastic Materials within the Framework of Finite-strain Elastoplasticity. In. Engineering Design Applications II: Structures, Materials and Processes. Eds. A. Öchsner and H. Altenbach, Springer, 2019 (In press).

[15] R. Jerábek, L. Écsi, Numerical Study of Material Degradation of a Silicone Cross-shaped Specimen Using a Thermodynamically Consistent Mooney-Rivlin Material Model, Novel Trends in Production Devices and Systems V, Materials Science Forum. 952 (2019) 258–266.

[16] M.A. Crisfield, Non-linear finite element analysis of solids and structures, Essentials, Vol. 1, John Wiley & Sons Ltd., Chichester, 2000.

[17] L. Écsi, P. Élesztős, R. Jerábek, R. Jančo, B. Hučko, An Alternative Framework for Developing Material Models for Finite-Strain Elastoplasticity, IntechOpen Ltd., London, DOI: 10.5772/intechopen.85112, 2019.

[18] K.B. Putra, J. Plott, A.J. Shih, Biaxial Mooney-Rivlin coefficient of silicone sheet by additive manufacturing, Procedia CIRP. 65 (2017) 189–195.